# Vanadium Redox Flow Battery Electrode Derived from Electrodeposition of a Copper-based Metal-Organic Framework onto Lead Dioxide

Michael Barta

A thesis

submitted in partial fulfillment of the

requirements for the degree of

Master of Science in Materials Science and Engineering

University of Washington

2019

Committee:

Guozhong Cao

Chaofeng Liu

Program Authorized to Offer Degree:

Materials Science and Engineering

University of Washington

## Abstract

Vanadium Redox Flow Battery Electrode Derived from Electrodeposition of a Copper-based Metal-Organic Framework onto Lead Dioxide

Michael Barta

Chair of the Supervisory Committee:

Professor Guozhong Cao

Materials Science and Engineering

Metal-organic frameworks (MOFs) are metal-cation-containing structural building units connected into crystalline nets via organic linkers, and they often possess high surface area and coordinatively unsaturated metal ions, both features that make MOFs appealing candidates for electrochemical applications. Vanadium redox flow batteries (VRFBs), which hold promise for use in stationary grid-level electrochemical energy storage, are one such area of potential application that may serve to benefit from the properties of MOFs.
Enhancing the redox kinetics of the $VO^{2+}/VO_2^{+}$ reaction at the positive electrode of the VRFB can improve the power capabilities and cycle life of the battery. The extensive porosity of MOFs can serve to increase the reactive surface area of current VRFB electrodes and potentially offer a greater number of catalyst sites by means of oxygen functionals inherently present in MOFs. Lead dioxide electrochemically deposited on carbon felt is used as a substrate for electrochemical deposition of a well-known Cu-based MOF. Subsequent pyrolysis of the coated carbon felt and placement in a VRFB half-cell yields results that suggest more facile electrode kinetics and performance that matches or exceeds several other treated electrodes mentioned in current literature. Consequently, the evidence indicates that MOF-derived structures on carbon felt have significant potential to improve overall VRFB performance.

## Table of Contents

# 1. Introduction

While the search for new and better materials is perpetual in academia and industry, the continually magnifying effects of climate change have made that search all the more urgent, as governments and organizations seek to combat climate change or improve sustainability meaningfully but also in a way that is cost-effective.[1, 2] Part of the challenge of reducing or even reversing the negative effects climate change is reducing or eliminating anthropogenic carbon dioxide emissions from fossil fuel use, emissions which alarmingly have been observed still to be steadily increasing globally according to recent data.[3] Replacement of fossil fuels as an energy source by renewable sources, like wind or solar, is essential, but these sources of clean energy are not without their own drawbacks; for instance, by relying on nature these sources can provide energy only intermittently. As a result, efficient energy storage—especially in the form of batteries, supercapacitors and more—is a crucial element of the renewable energy implementation and success.[4, 5]

One particularly promising form of electrochemical energy storage is the vanadium redox flow battery (VRFB). Originally proposed by Skyllas-Kazacos in the 1980's, the system relies on the versatile vanadium cation and its many oxidation states to generate a battery cell potential.[6, 7] Electrochemical reactions for the VRFB are heterogenous, occurring at the interface between the solution and a battery electrode. As such, the electrode's surface area, pore size distribution, and catalytic characteristics of the battery's electrode become an important parameter for the overall performance and robustness of VRFBs. As a result, materials that offer the opportunity to tailor these surface properties are highly desirable; metal-organic frameworks offer just such an opportunity.

Metal-organic frameworks (MOFs) are a relatively new class of materials, but they have been studied extensively in recent years. Though more than 20,000 varieties of MOF have been reported since 2003, [8] their general building blocks are the same: formally cationic units containing a metal (*i.e.,* a structural building units, or SBUs) are connected by a network of organic, formally anionic units (i.e., polytopic linkers). [9] These units arrange themselves in a way that often leads to an open framework with relatively large accessible spaces within the crystal. In other words, many MOF's are extensively porous materials, and that porosity can be tailored.

With the help of a $PbO_2$ intermediate layer to aid HKUST-1 nucleation and the vanadium redox reaction, HKUST-1 is coated onto a lead dioxide coated carbon felt electrode (CF/$PbO_2$) and pyrolyzed. The resulting carbon structure on the electrode surface helps promote better kinetics for the VRFB positive electrode reaction.

# 2. Background

## 2.1 Metal-Organic Frameworks

Metal-organic frameworks (MOFs), though encountered previously, saw renewed interest in the 1990's, thanks in large part to the work of Kitagawa, Yaghi, and others. [10, 11, 12]

MOFs consist of metal, or metal containing, centers commonly referred to as secondary-building units (SBUs) connected via organic linkers. Because the crystal structure of the MOF is determined by the geometry and connectivity of the linkers (ditopic, tritopic, etc.) as well as that of the SBU's, the mathematical field of graph theory has informed much of what types of structures, or "nets", are mathematically possible given restrictions on connectedness. [13] And

though certain structures may be deemed mathematically possible, however, they still may not be chemically possible. These nets often lead to wide spaces within the structure, giving large surface areas, and in one case even a world record 7800 $m^2/g$. [14]

The coordination environment of the metal in the SBU influences its reactivity with other molecules introduced into the structure. This means the MOFs can be chemically selective , for instance, during gas separation. Additionally, the pore size may be controlled to the extent that small pores are created to physically sieve larger gas molecules like $CO_2$, $N_2$, and others. [15]

Bonding within MOFs is a mix, with covalent bonding within the organic linker and coordinative bonding between the metal cation and its neighbors. The strength of that metal-ligand bond is important for chemical stability, yet many MOF's have poor chemical stability, particularly against water. [16] Essentially, metal-ligand bond strength follows the Pearson principle of hard/soft acid/base combinations (HSAB); hard acids bond strongly with hard bases and soft acids bond strongly with soft bases. Metal-ligand bond strength increases with more acidic metal and more basic ligand. Cations of high charge density, like $Zr^{4+}$, bond strongly with, for instance, carboxylates. [17] Cations of low charge density and with a more deformable electron bond strongly with weak bases, like azolates. Water stability can also be improved via kinetics, like methyl groups on the ligand shielding the metal-SBUs from water

The appeal of MOF also stems from their tunability; they can be changed in any number of ways. One common approach to enhancing pore size is to apply organic linkers of extended length, in which case the topology of the original MOF remains but the crystal pore size increases because of the larger organic molecules in place. [18] This area of MOF manipulation is considered (iso)reticular synthesis. The limitation of this approach is that the risk of structure

interpenetration increases with linker length and interpenetration effectively occupies the space desired for larger pores.

Another way to tailor the MOF structure is by direct modification of its inherent chemistry. Post-synthetic modification (PSM) refers to the direct alteration of a MOF crystalline solid (*e.g.*, introduction of new ligand functionality) by way of a heterogeneous chemical reaction. In other words, one starts with a porous MOF that possess linkers amenable to modification and that is stable under the reaction conditions, and then one uses solution chemistry to alter or add functional groups to the existing MOF structure. [19] Conceivably, this method could be used to change the reaction environment possible within a MOF, like whether a pore is hydrophilic or hydrophobic. Also, just as ligands can be exchanged, so too can the original cations be exchanged, for even greater manipulation of pore chemistry and catalysis. [20, 21]

MOFs can be prepared in several ways, including solvothermal (most common), [22] electrochemical, [23], microwave-assisted, [24] and mechanochemical routes. [25] For industrial scalability, some methods are better than others. Electrochemical and mechanochemical synthesis of MOFs have an advantage in terms of scalability, and indeed these methods have been put to use for production of MOFs at an industrial scale. [26, 27] The German chemical company BASF produces an aluminum MOF and they were the first to devise an electrochemical route for synthesis of the Cu-based MOF, HKUST-1 (name after Hong Kong University of Science and Technology, which is credited with its original creation). [28]

Occasionally, the pore and polygonal structure may be retained even after pyrolysis of the MOF. Young *et al.* used a common Zn-based MOF, ZIF-8 (zeolitic imidazolate framework) as a carbon source to make microporous/mesoporous carbon that retained ZIF-8 polygonal

structure even after applying temperatures of 800°C-1000°C for graphitization. [29] The materials heated to 900°C showed the best performance and were superior to activated carbon in several electrochemical tests. Retention of the carbon pore structure after pyrolysis further increases the application flexibility of MOFs.

## 2.2 Vanadium Redox Flow Batteries

**Schematic 1** provides the general arrangement of the components of a vanadium redox flow battery.

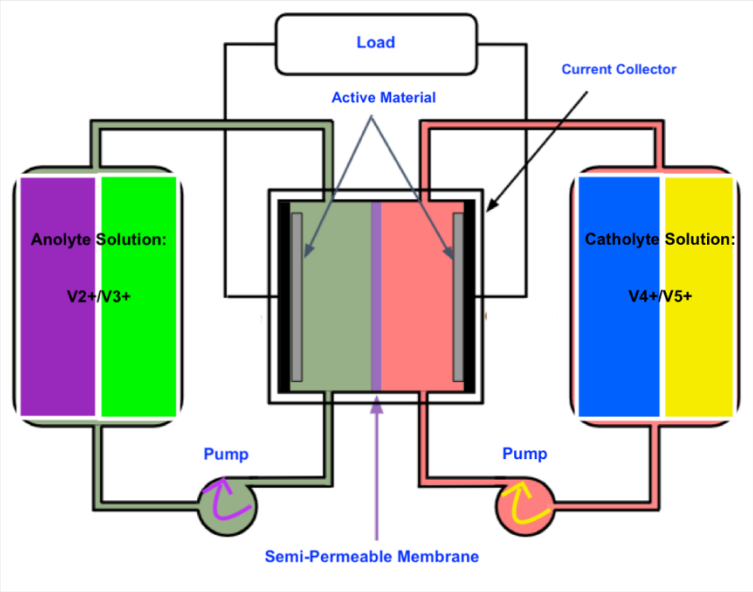


***Schematic 1**. Components of a Vanadium Redox Flow Battery*

A vanadium redox flow battery (VRFB) relies on the $V^{2+}/V^{3+}$ and $V^{4+/}$ $V^{5+}$ redox reactions to generate a voltage. The standard reduction potential for each couple is given in Eq.1 & Eq.2. During discharge, anolyte solution is pumped over the negative electrode and the $V^{2+}$ in solution oxidized to $V^{3+}$. On the other side, catholyte solution is pumped over the positive

electrode and $VO_2^+$ (i.e., $V^{5+}$ ) is reduced to $VO^{2+}$ (i.e., $V^{4+}$). Ideally, only hydronium ions pass thru the semi-permeable membrane to balance charge. The pumps are powered by the battery itself. Typically, both solutions have some concentration of sulfuric acid, but additives are likely also present.

$$VO_2^+ + 2H^+ + e^- \leftrightarrows VO^{2+} + H_2O \qquad E° = 1.0\,V\ (vs\ SHE) \qquad (1)$$

$$V^{3+} + e^- \leftrightarrows V^{2+} \qquad E° = -0.26\,V\ (vs.SHE) \qquad (2)$$

The interesting aspect of the VRFB is that unlike, say, Li-ion battery systems, the capacity and power of a VRFB are decoupled. In other words, because the redox active species are not stored in the electrodes themselves, the amount capacity (i.e., the volume of electrolyte and electrolyte concentration) and the electrode active surface (i.e., stack size) can be varied independently, depending on need. [30]

There are several other advantages to VRFBs systems, like their portability, capability for deep discharge, and high cycle life; [31] however, there is still room for improvement, particularly in catalyzing redox reactions at both the positive and negative electrodes, and research continues in this regard. [32, 33]

## 3. Motivation

Mesoporous carbons have been shown to improve kinetics of the vanadium redox reaction and improve flow battery performance. [34] The porosity of the MOFs, like HKUST-1 may offer the same advantages but with easier and cheaper synthesis. Electrodeposition is fast and scalable,

especially when compared to the common yet slower solvothermal methods of MOF preparation. The large surface area and unsaturated coordination environment of metal ions inherent to many MOFs make them appealing materials for use in areas requiring fast heterogeneous reactions, like catalysis. The ability to grow MOF-based thin films on various substrates is highly desirable, but research of MOFs or MOF-derived material growth onto carbon electrodes for use in VRFBs is limited. It has been demonstrated that HKUST-1 has an affinity for nucleation on certain metal oxides, [35] and HKUST-1 is a well-known MOF with myriad relatively simple synthesis methods, including electrochemical methods.

# 4. Methods

## 4.1 Materials

As the carbon felt substrate, SGL Group's Sigracell battery felt, a graphite felt synthesized from polyacrylonitrile (PAN), was chosen. ACS grade chemicals purchased from Sigma Aldrich include lead(II) nitrate [ $Pb(NO_3)_2$ ], copper(II) nitrate hemipentahydrate [ $Cu(NO_3)_2 * 2.5 H_2O$ ], vanadium(IV) oxide sulfate hydrate [ $VOSO4 * xH_2O$ ], and trimesic acid [ $C_6H_3(CO_2H)_3$ ]. Nitric acid [ $HNO_3$ ] , sulfuric acid [ $H_2SO_4$ ], glacial acetic acid [ $CH_3COOH$ ], and anhydrous methyl alcohol [ $CH_3OH$ ] were purchased from Macron Fine Chemicals. Copper (II) chloride dihydrate [ $CuCl_2 * 2H_2O$ ], sodium acetate [ $CH_3COONa$ ], lead(II) acetate [ $(CH_3COO)_2Pb$ ], copper foil, anhydrous ethanol [$C_2H4_5OH$], and boric acid [ $H_3BO_3$ ] were all purchased from Alfa Aesar. All chemicals were used as received, without any further refinement or purification.

## 4.2 Synthesis

### 4.2.1 Carbon Felt Acid Treatment

The SGL carbon felt is received in large sheets and so were first cut into pieces of dimensions 7 x 5 x 1 mm. Carbon felt pieces were then placed in a solution 50% v/v sulfuric acid solution, which was then sonicated for 1 h and stored for 8 h. At the end of 8 h, the carbon felt was rinsed repeatedly with water to remove any remaining sulfuric acid and then dried in a drying oven at 70 °C in air for 4 h.

### 4.2.2 $PbO_2$ Electrodeposition

Three different lead-ion baths were used to electrodeposit $PbO_2$ onto ATCF, with each bath and set of deposition parameters leading to a different observed morphology.

In the first method, the acid-treated carbon felt (ATCF) served as an anode and cathode in a lead nitrate (81.0 mM) and nitric acid ( 1M ) aqueous solution and two-electrode deposition cell. A dc-power supply was then used to apply a pulse-deposition. While stirring, a constant current of 300 mA was applied for three seconds on, and removed for ten seconds. This constituted one cycle. Five cycles were applied for one electrode.

In the second $PbO_2$ deposition method, ATCF served as anode and cathode in a lead nitrate ( 9.2 mM ) and boric acid ( 0.728 M ) solution and two-electrode cell. A current density of 5 $mA/cm^2$ was applied for 1 h while the solution was stirred.

In the third $PbO_2$ deposition method ATCF again served as anode and cathode. The aqueous solution consisted of lead(II) acetate ( 1M ), sodium acetate ( 1M ), and acetic acid ( 1M ). A current density of 2 $mA/cm^2$ was applied for 1 h while the solution was stirred.

In each case, after deposition was complete, the anode with the formed $PbO_2$ was immediately rinsed copiously amounts of DI water before use as substrate. For any characterization, after rinsing the electrode was dried in air at 75°C for 3-4 hours.

### 4.2.3 HKUST-1 Deposition

The HKUST-1 metal organic framework was electrochemically deposited onto the lead dioxide-coated ATCF ( ATCF/$PbO_2$ ) from one of two possible synthesis baths. In preparation of the first bath, $Cu(NO_3)_2$ * 2.5 $H_2O$ was dissolved in DI water for a molarity of 0.172 or 0.107 , while trimesic acid was dissolved in ethanol for a resulting molarity of 0.1 or 0.125. The two solutions were then combined; this first HKUST-1 synthesis solution is designated HSS1. For a particular temperature and deposition time, a constant potential was applied to a deposition cell consisting of a ATCF/ $PbO_2$ cathode (working electrode, WE) and Cu metal anode (counter electrode, CE), after which the working electrode was immediately rinsed with DI water and ethanol. After rinsing, the electrode was dried in air for 3-4 hours.

The second synthesis solution, designated HSS2, is similar to the first except that copper nitrate is replaced by copper chloride dihydrate and ethanol is replaced by methanol.

### 4.2.4 Pyrolysis

For pyrolysis, electrode samples were heated in a tube furnace. At 10 °C/ min and under nitrogen gas flow, the sample was heated to 500 °C, a temperature at which it remained for 10 h. The sample was then allowed to cool naturally back to room temperature.

## 4.3 Structural Characterization

### 4.3.1 XRD

To obtain phase and structural information, each sample was characterized using x-ray diffraction (XRD) patterns. XRD scans were performed at ambient temperature on a Bruker D8 Discover powder diffractometer using Cu anode x-ray source (Cu *K-α* wavelength = 1.5406 Å) and collimated beam geometry (0.5 mm collimator & 10.5 mm slit width) with a 2D detection system. For a typical scan, 2θ = 5° - 83°, samples were rotated during data collection to improve sample statistics, and a wind screen was applied to reduce noise from air scattering. 2D scan information was integrated and converted to 1D spectra using Bruker's Diffrac.EVA software, then material phases were identified using JADE XRD analysis software. To determine phase and weight fractions for each sample, Rietveld analysis was performed using the freely available opensource software GSAS-II [36].

### 4.3.2 SEM/EDS

Sample morphology was characterized via scanning electron microscopy (SEM), and in addition, information about element identity, distribution, and relative quantity was gained from energy dispersive spectroscopy (EDS). Two pieces of equipment were used, each with SEM/EDS capability: Sirion FEI XL30 with accompanying Oxford energy dispersive x-ray spectrometer, and JEOL JSM-6010 Plus. When necessary to improve imaging, nonconductive samples were carbon coated or sputter coated with Au & Pd.

### 4.3.3 TGA

To understand sample and phase thermal stability, thermogravimetric analysis (TGA) was performed. For typical analysis, a sample was heated to 1000 °C from ambient temperature at a rate of 10 °C /min under flow of nitrogen gas.

## 4.3 Electrochemical Characterization

### 4.3.1 Cyclic Voltammetry

While the bare portion of the working electrode was sandwiched between a Pt current collector and a Teflon support via a Teflon screw, the portion of the ATCF with active material protruded from the bottom of the holder and into the solution. The vanadium redox solution consisted of 0.25 M VOSO4 and 1 M of $H_2SO_4$ . For the remaining electrodes of the three electrode cell, the counter electrode was platinum foil and the reference electrode was a Ag/AgCl electrode. Typically the half-cell was cycled, beginning at open circuit voltage, between 0.1 and 1.7 V (vs. Ag/AgCl), at various scan rates.

### 4.3.2 EIS

Electrochemical Impedance Spectroscopy (EIS) was performed in a three-electrode cell at room temperature on a Solartron Impedance Analyzer. The active material on ATCF served as the working electrode, Pt served as the counter electrode, and Ag/AgCl served as the reference electrode. At the cell's open circuit potential, impedance spectra were obtained at applied frequencies between $10^{-2}$ to $10^{5}$ Hz at an amplitude of 10mV.

## 4.4 Experiment Design

In order to map out the effect of various synthesis parameters on the HKUST-1 nucleation and growth onto the $PbO_2$ coating, elements of $2^k$ factorial design were introduced. Specifically,

four factors, each with a high (+) and low (-) value, were chosen and a design matrix was used to consider all 16 combinations of factors (**Table 1**). The four factors chosen were voltage (-1.0 V & -1.5 V, vs. counter electrode), temperature (HSS1: 70°C & room temperature; HSS2: 60°C & room temperature), deposition time (10 min. & 5 min.), and solvent mol ratio (Ethanol/Water: 1.16 & 0.58; Methanol/Water: 1.68 & 0.84 ). For comparison, factor combinations were correlated with phase fraction results from Rietveld refinement of synthesized electrodes when possible.

***Table 1**. First Eight Tests of the Factorial Design Matrix*

| Test # | V | Temp. | Dep. Time | Solvent ratio |
|---|---|---|---|---|
| 1 | + | + | + | + |
| 2 | - | + | + | + |
| 3 | + | - | + | + |
| 4 | - | - | + | + |
| 5 | + | + | - | + |
| 6 | - | + | - | + |
| 7 | + | - | - | + |
| 8 | - | - | - | + |

# 5. Results

## 5.1 Structure and Morphology

In addition to good fairly good coverage of the carbon fibers, the three different $PbO_2$ electrodeposition methods led to three different morphologies (**Fig. 1**) and slight phase variations (**Fig. 2**). Lead dioxide deposition Method 1 yielded a surface morphology with the appearance nanometer-sized "rice grains". Method 2 yielded a relatively smooth surface, while method three yielded an undulating surface.

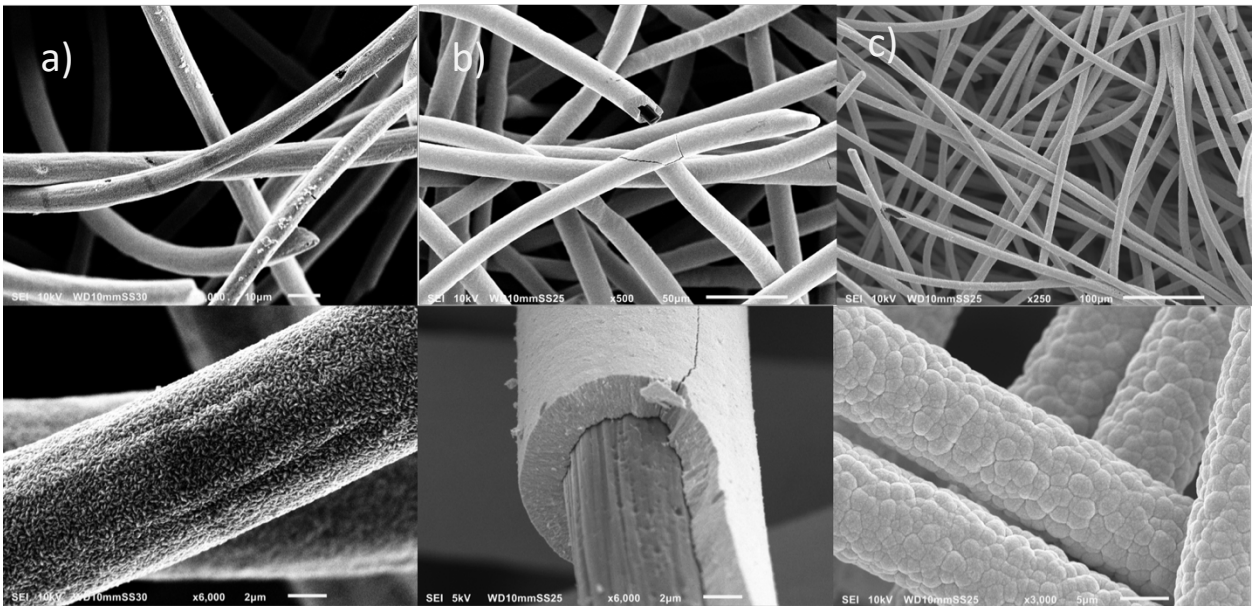


***Figure 1.*** *SEM of PbO2 electrochemically deposited onto acid-treated carbon felt using three different methods. a) Method 1, b) Method 2, and c) Method 3.*

The most common phase of $PbO_2$ encountered is the β- $PbO_2$ form, while the α- $PbO_2$ form is less common. XRD spectra of each method indicate that the ration of phases also varies with

method. The phase and weight fraction resulting from Rietveld refinement each method spectrum is given in **Table 2**.

The affinity HKUST-1 nucleation for of each type of $PbO_2$ surface was tested by submerging each coated electrode into HKUST-1 synthesis solution 1 (HSS1). From SEM observations (**Fig.3**), HKUST-1 polyhedra appear on the surface from Method 1, but hardly at all on the other $PbO_2$ surfaces. Because of the apparent preference for nucleation on the surface from $PbO_2$ from Method 1, as well as Method 1's quicker deposition time ( < 2min.), it was chosen as the primary substrate for later HKUST-1 deposition.

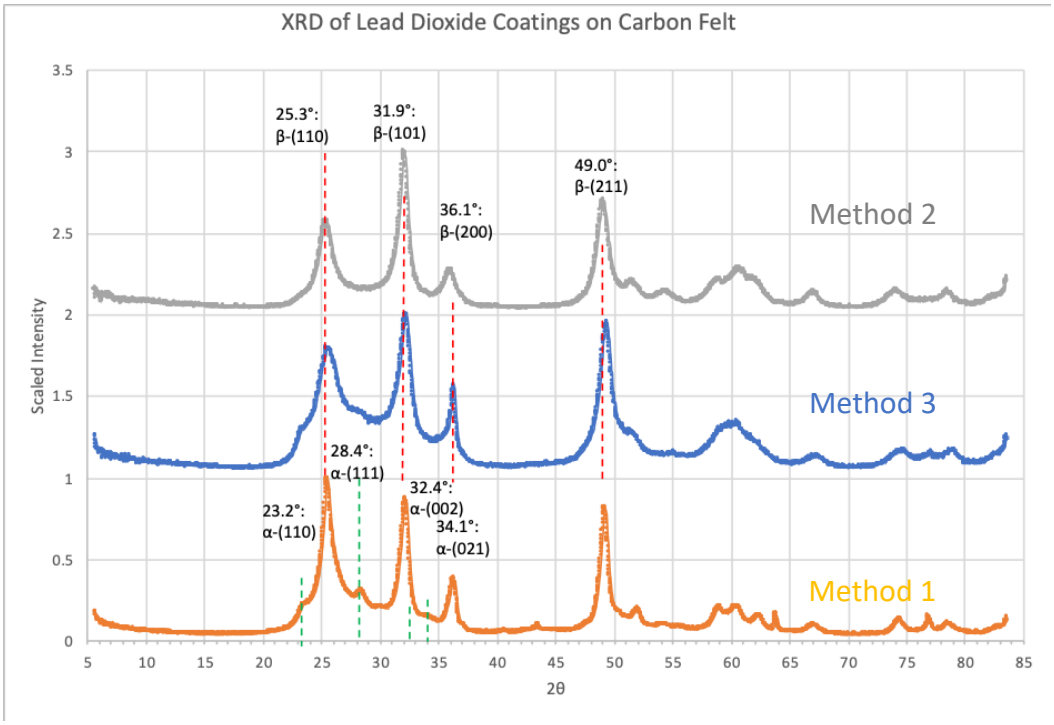


***Figure 2**. XRD of the three different methods of lead dioxide coating onto carbon felt. Primary peaks for each lead dioxide phase are indicated. The max intensity for each spectrum has been scaled to 1. Two spectra have been shifted upwards for clarity.*

***Table 2.*** *Phase and Weight Fractions of Lead Dioxide Determined by Rietveld Refinement*

| | Method 1 | | Method 2 | | Method 3 | |
|---|---|---|---|---|---|---|
| | α | β | α | β | α | β |
| Phase Fraction | 0.126 | 0.874 | 0.061 | 0.939 | 0.224 | 0.776 |
| Weight Fraction | 0.224 | 0.776 | 0.181 | 0.819 | 0.443 | 0.557 |

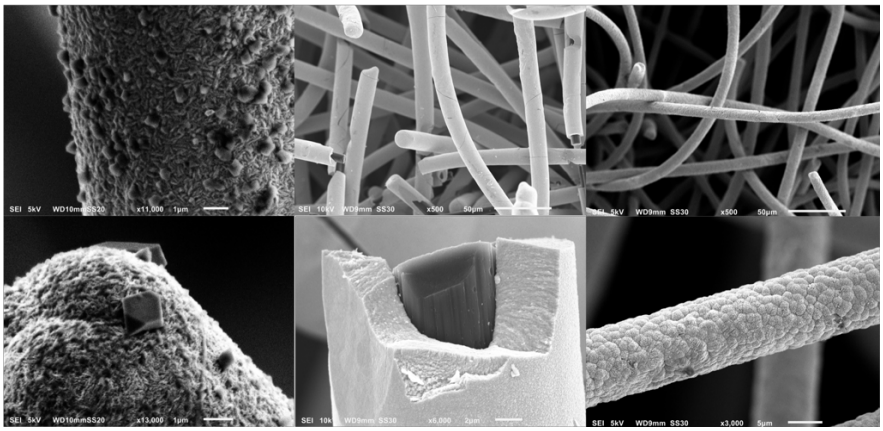

***Figure 3.*** *SEM images of lead dioxide coated carbon felt after soaking in HSS1 for 10 min.*

A $2^4$ factorial design matrix yielded 16 different combinations of factors for each solution type (HSS1 & HSS2). A combination of SEM observations, XRD observations and Rietveld analysis, was used to roughly determine degree of HKUST-1 coverage and lead dioxide integrity. Interestingly, the greatest degree of coverage came from Tests 3 both HSS1 and HSS2; diffractograms, phase fractions, and SEM images are similar for each (**Fig.4**)

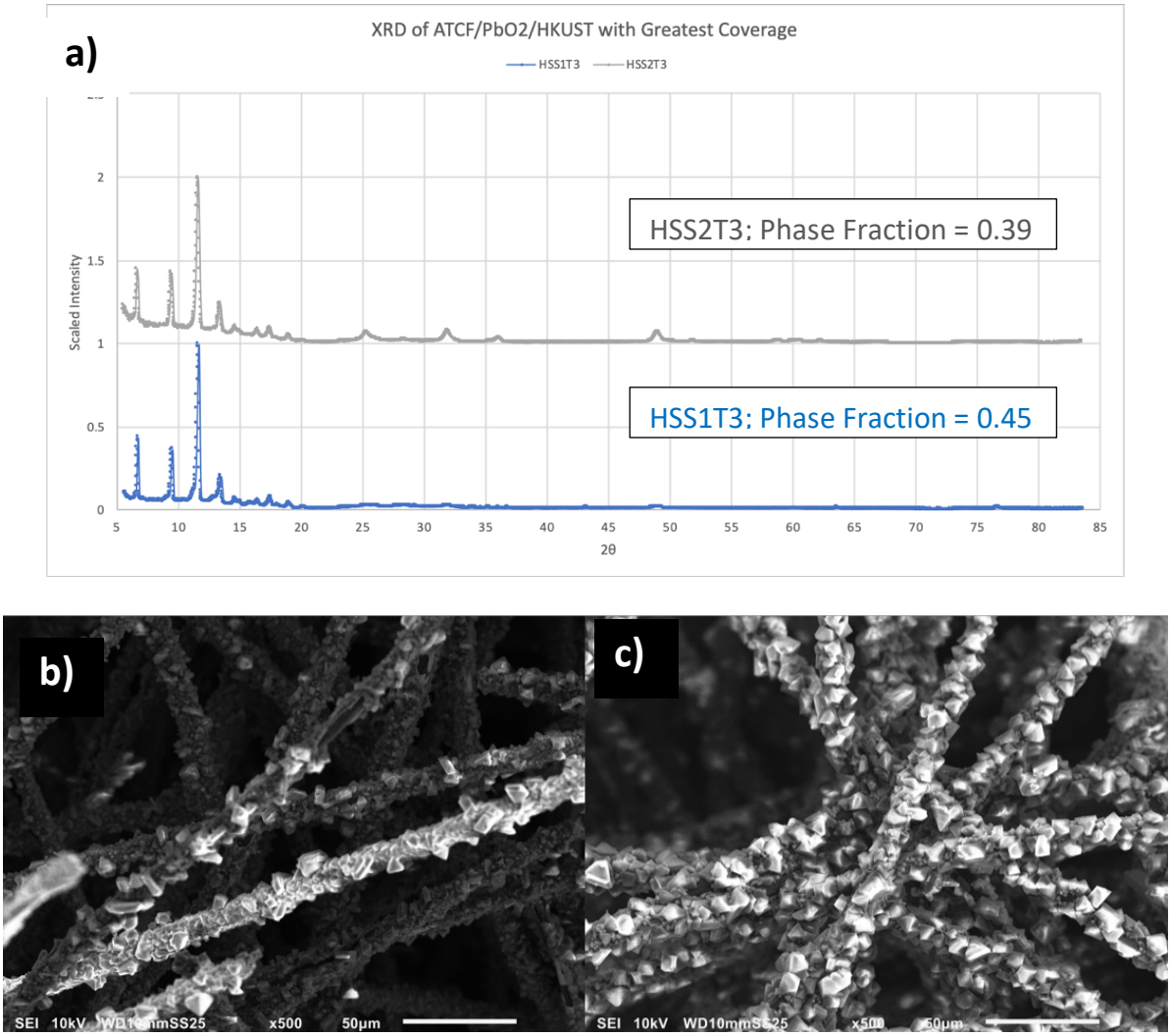


***Figure 4.*** *a) XRD and phase fractions of ATCF/PbO2/HKUST with greatest coverage. Maximum intensities are scale to 1, and some diffractograms are shifted for clarity. SEM of b) HSS1T3 and c) HSS2T3*

In Fig.4, visible are the characteristic diffraction peaks of HKUST-1 occurring at 2θ = 11.7°, 9.5°, 6.7°, and 13.5° for (hkl) planes (222), (220), (200), and (400) respectively. [37] The characteristic diffraction peaks for β-PbO2 are also present at 2θ = 25.3°, 21.9°, 36.1°, 49.0°.

For use as an electrode in a VRFB half-cell sample HSS1T3 was pyrolyzed at 500 °C for 10 hours under flow of nitrogen. TGA of a ATCF/$PbO_2$/HKUST sample and, for comparison, HKUST-1

powder synthesized from the same solution revealed the mass changes that occurred during pyrolysis (**Fig. 5**) The curves overlap up to 50°C during water loss, but after 50°C, the HKUST-1 powder continued to lose more water, while the coated electrode plateaued. HKUST-1 degradation occurred at about 300°C for the powder but just before 350°C for the electrode, though the mass loss for the electrode due to HKUST-1 loss is less simply because there is less HKUST-1 on the electrode compared to the pure powder. Shortly after 350°C, $PbO_2$ also degrades, reduced to PbO and Pb metal as oxygen leaves the system.

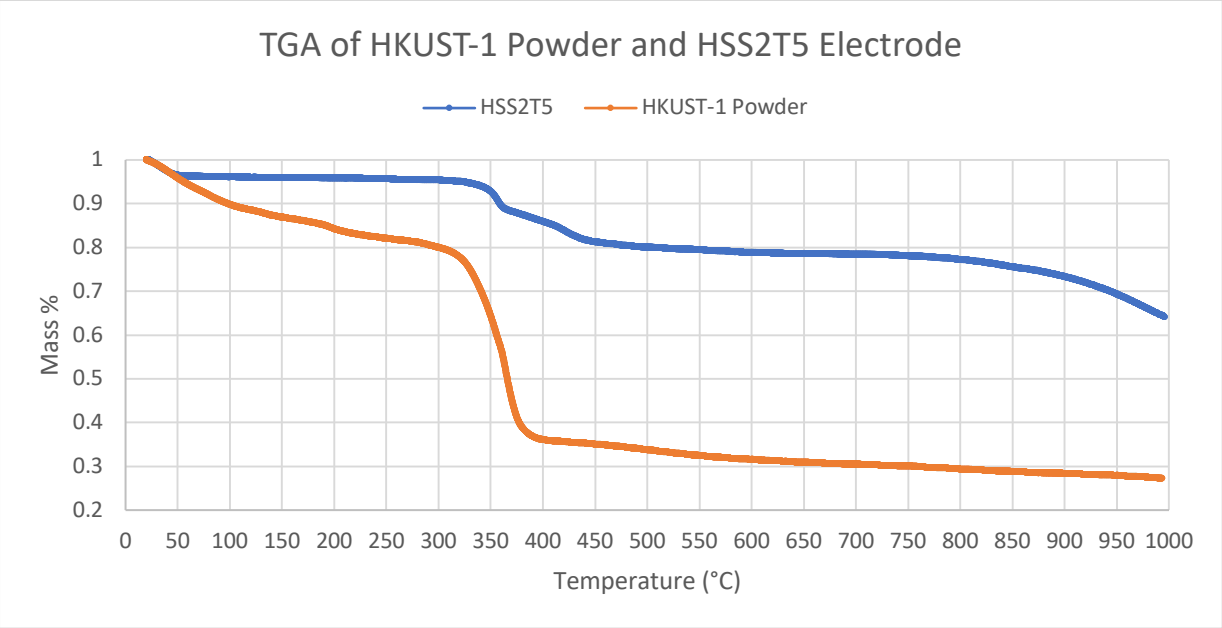


***Figure 5**. TGA of HKUST-1 synthesized powder and HSS2T5*

The products of pyrolysis, as evidenced in the diffractogram of the electrode (**Fig. 6**), include PbO {2θ= 29.0° (111), 2θ= 30.2° (020), 2θ= 32.5° (200), 2θ= 37.7° (201)}, Pb {2θ= 31.1° (111),

2θ= 36.1° (200), 2θ= 52.1° (220), 2θ= 62.0° (311)}, Cu {2θ= 43.3° (111), 2θ= 50.4° (200)}, and carbon {2θ= 25.1° (002)}.

The SEM micrograph of the sample after pyrolysis shows bead-like structures in the nanometer to micron size range, which are confirmed by EDS to be Cu and Pb metal, along a bed of carbon remnants of the original HKUST-1 polyhedra (Fig. 6, inset).

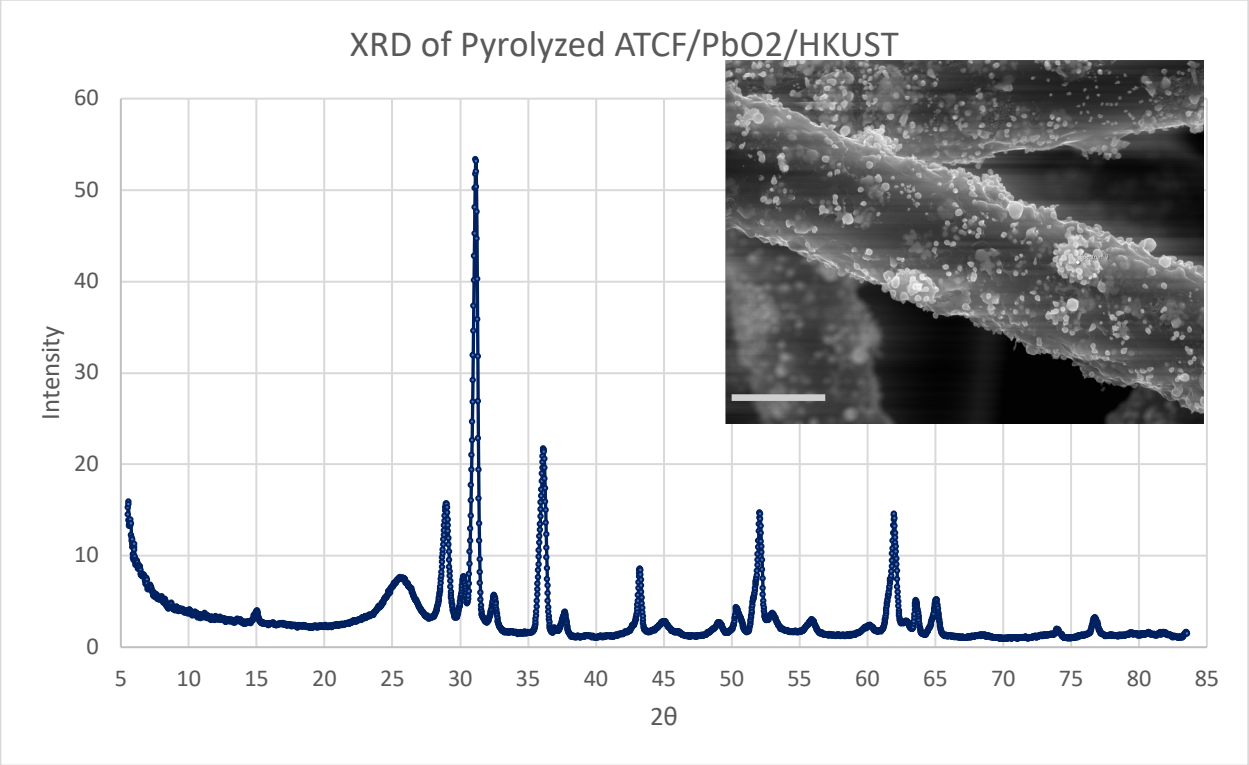


***Figure 6**. Diffractogram of HSS2T3 after pyrolysis. Inset is SEM micrograph of HSS2T3 after pyrolysis. Scale bar is 5 microns.*

## 5.2 Electrochemical Characterization

The pyrolyzed HSS1T3 (HSS1T3Py) was used as the positive electrode in a VRFB half-cell for cyclic voltammetry, along with a platinum counter electrode and Ag/AgCl reference electrode;

**Fig. 7** shows the resulting curve, as well as curves for the same test but with other positive electrodes too, like plain ATCF, and ATCF/$PbO_2$ , while **Table. 3** shows the calculated peak differences ($\Delta E_{pc}$), and anodic/cathodic peak ratios ($I_{ap}/I_{cp}$). Notably, HSS1T3 possesses the smallest peak difference and the peak ratio closes to 1 both values being a metric for reversibility of the reduction-oxidation reaction at the electrode surface. [38]

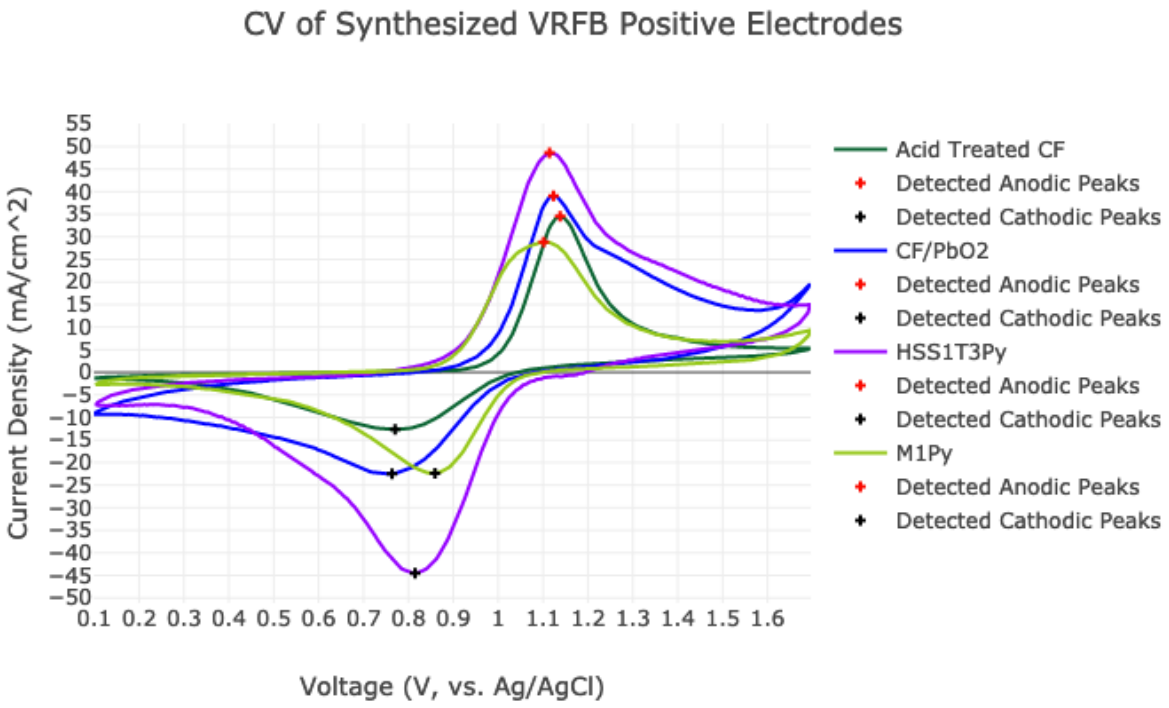


***Figure 7.*** *Cyclic voltammogram of synthesized electrodes.*

***Table 3**. Peak Differences and Peak Current Ratios from CV curves.*

| Sample ID | ATCF | CF/$PbO_2$ | HSS1T3 | M1Py |
|---|---|---|---|---|
| $\Delta E_{pc}$ (V) | 0.37 | 0.36 | 0.3 | 0.24 |
| $I_{ap}/I_{cp}$ | 2.7 | 1.7 | 1.1 | 1.3 |

# 6. Discussion

## 6.1 Role of Carbon Felt Surface

Before immersing the carbon felt (CF) electrodes in a deposition solution, the CF should be treated. Untreated carbon felt is hydrophobic, and poor wetting of the electrode surface in the VRFB aqueous solution hinders reactions. However, introducing oxygen functional groups (i.e., carboxylic, phenolic, etc.) to the surface—via heat, chemical, or electrochemical treatment—has been shown to counteract this phenomena and improve carbon surface's electrochemical activity and wettability. [39, 40] For example, when testing at ambient temperatures the effect of various heat treatments of carbon felt of VRFB negative half cells, Langner et al. observed a significant reduction in overpotential in the heat treated CF compared to the untreated felt, which led to an improvement of cell voltage efficiency of 10-19%. [41] Additionally, treatment of carbon felt in sulfuric acid has been showed a discernible increase in oxygen functional groups on the surface, making it hydrophilic. [42] In general, different treatments lead to different surface concentrations of the various oxygen functional groups. Here acid treatment's primary purpose was as a basic and relatively quick way to increase CF activity, [42] and serve as the standard against which other electrodes could be compared.

## 6.2 Role of $PbO_2$ Surface

In solution, metal oxides tend to acquire a surface charge, be it through de/prototation of surface oxygen atoms or the loss of surface species, and the pH at which the charge on the surface is neutral is known as the isoelectric point (IEP). HKUST-1 has shown an affinity to nucleate on metal oxide surfaces of high IEP without and applied potential, such as ZnO and CdO, where the basicity of the metal oxide surface may aid in deprotonation of the organic linker in solution and its anchoring to the oxide surface. [43, 35] Lead dioxide has been observed having an IEP > 8, meaning that in solutions of pH less than 8, the surface of lead dioxide is positively charged. [44] From SEM images in Fig. 3, HKUST-1 appears to show a slight preference for nucleation on the PbO2 electrodeposited using Method 1. It's unclear from literature how the alpha and beta phase fractions of $PbO_2$ might affect the isoelectric point, and here how the phase fraction might affect nucleation if at all, but morphology may also play a role. The "rice grain" morphology of Method 1 likely possess a higher surface energy due to the smaller radius of the surface particles, compared to the other deposition methods, which are relatively smoother.

## 6.3 HKUST-1 Electrodeposition

Electrodeposition of HKUST-1 may be divided into two categories: anodic deposition and cathodic deposition.

Electrodeposition is a technique of MOF synthesis that is less often used than others, like solvothermal methods. There are generally two types of electrodeposition for MOFs: anodic deposition and cathodic deposition. In the cathodic process, the metal cation is in solution with the organic linker. The pH of the bulk solution is high enough to suppress dissociation of the

linker's acid form and therefore formation of MOF particles in the bulk. Li and Dincă show that when the potential of working electrode in solution is low enough and there is a probase in solution, like $NO_3^-$ or triethylammonium ($Et_3NH^+$), is electrochemically reduced, leading to more basic species, and the pH of the region near the electrode is then increased; the pH gradient between the solution near the electrode and the bulk solution promotes linker dissociation and, consequently, MOF formation near the electrode. [45, 46]

In the anodic electrodeposition process, the metal cation source is not the solution but the electrode itself. For the synthesis of HKUST-1, the working electrode is Cu metal and the organic linker is in solution with supporting electrolyte. An anodic potential is applied to Cu, and Cu2+ dissolve into solution near the surface, where once the concentration of cations is high enough HKUST-1 nucleates. [47, 48] In both the cathodic and anodic deposition processes, important parameters to consider in MOF electrodeposition include applied potential, current density, distance between electrodes, pulse time, synth. time, solvent, linker, and electrolyte concentration, [49] many of which were used as factors in the design matrix to map deposition of HKUST-1 onto the CF/$PbO_2$ electrode.

In trying to achieve a fairly even coating of HKUST-1 on CF/ $PbO_2$ it became more likely that the process of HKUST-1 deposition onto $PbO_2$ is likely slightly different from other well-known electrodeposition processes. When depositing from the more typical solution EtOH/H2O/CuNO3, the negative potential applied to the CF/PbO2 electrode induced HKUST-1 at the surface, but also Cu metal deposition and HKUST-1 formation in solution, presumably due to $PbO_2$ particles entering solution and providing nucleation site for organic linker. Examples of Cu metal deposition and $PbO_2$ break-off during synthesis in HSS1 are shown in **Fig.**

**8**. We see the primary Cu metal XRD peaks present at 2θ = 43° and 50°, as well as no discernible $PbO_2$ peaks.

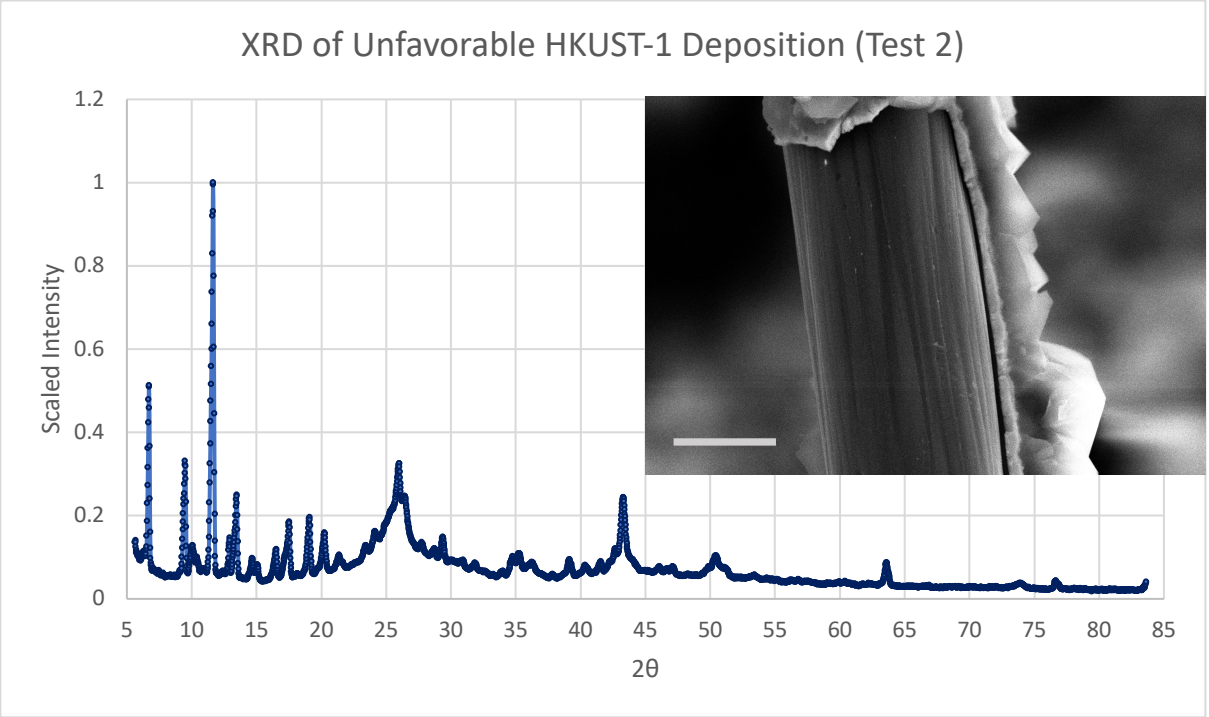


***Figure 8**. XRD showing Cu deposition along with significant loss of lead dioxide. Inset show SEM image of lead dioxide break-off during deposition. Scale bar is 5 microns.*

If $PbO_2$ was electrochemically dissolving in solution, there are a couple possible reactions occurring.

$$PbO_2 + 4H^+ + 2e^- \leftrightarrow Pb^{2+} + 2H_2O \quad (3)$$

$$PbO_2 + H_2O + 2e^- \leftrightarrow PbO + 2OH^- \quad (4)$$

PbO is not observed in any of the XRD diffractograms, leading one to believe that Eq. 1 is more likely happening during HKUST-1 deposition. Both reactions have the effect of increasing pH near the electrode, which would induce HKUST-1 formation, similar to the cathodic reduction method. Despite the good result from HSS1T3, there was a question of whether dissolution could be controlled to better maintain $PbO_2$ integrity with less chance of Cu metal deposition and whether the nitrate ion was necessary for deposition. To try and answer these questions, methanol replaced ethanol and $CuCl_2$ replaced $CuNO_3$ for HSS2.

The chlorine anion served a number or different roles. At pH < 3, chlorine anions in solution accelerate PbO2 dissolution. [50] Furthermore, they allowed elimination of the possibility nitrate ion reduction at the working electrode as the source of any pH gradient, and they better stabilized $Cu^{2+}$ cations in solution, reducing the chance of Cu metal deposition on the working electrode, as well as HKUST-1 nucleation in the bulk solution. Without a nitrate ion present and no visible bubbles, signaling hydrogen gas evolution, forming at the cathode during synthesis, the belief is that lead dioxide reduction is the reaction by which the surface increases its pH to induce HKUST-1 formation. Also, the dissolution mechanics did indeed change, evidenced by the appearance of pore-like features in the $PbO_2$ surface (**Fig. 9**) that were not present in HSS1 solution deposition, and smaller HKUST-1 polyhedra were more likely in the HSS2 solution. Though Test 3's parameters led to the best coverage for HSS1 & HSS2 solution, noticeably the $PbO_2$ XRD peaks in HSST3 are of greater intensity and phase fraction, suggesting HSS2T3 maintained better $PbO_2$ integrity.

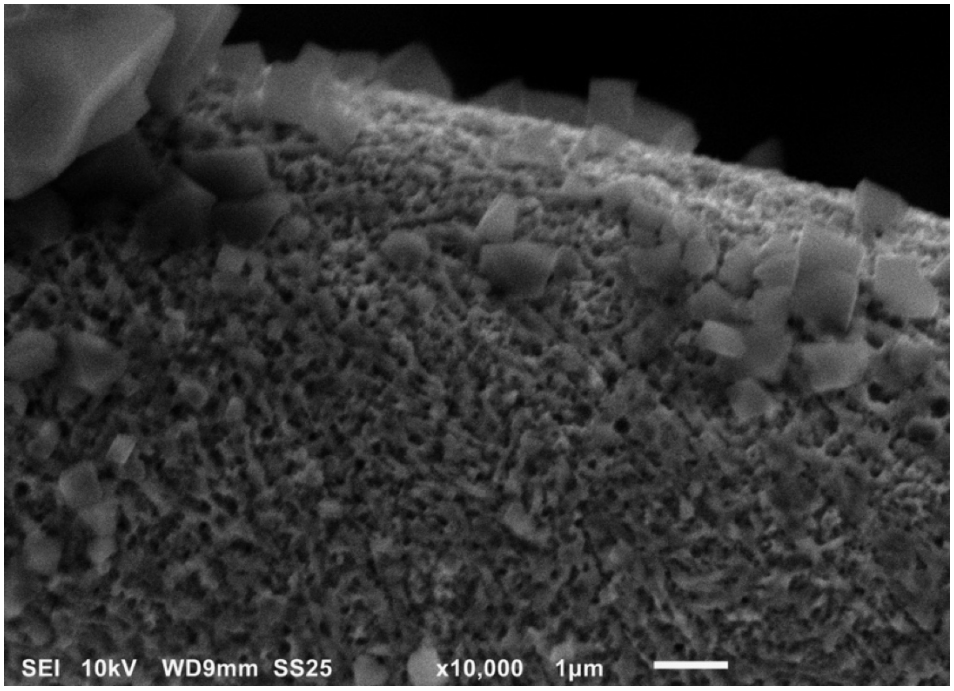


***Figure 9.*** *SEM Image of CF/$PbO_2$ surface after HKUST-1 deposition in HSS2.*

## 6.4 Pyrolysis

Pyrolysis of HKUST-1 powder and coated electrode yielded similar TGA results. Notably, though water loss overlaps for both materials, decomposition of HKUST-1 occurs at a slightly higher temperature when it is coated on CF/$PbO_2$., suggesting that its thermal stability is slightly improved as a film.

From Fig.6, Pyrolysis of HSS2T3 drastically changes the surface of the electrode. Song et al. pyrolyzed HKUST-1 powder and observed Cu nanoparticles embedded in a carbon matrix with recognizable polyhedral character, similar to the source MOF. [51] Here, pyrolyzing the Cu anode that was also present in the electrochemical bath for HSS2T3, yields a similar result (**Fig. 10**).

The Cu anode is actually simultaneously participating in HKUST-1 deposition via the anodic process outlined previously. Though both electrodes are made in the same bath, their pyrolysis yields different morphology. Upon closer inspection, there appear to be several instances of Cu nanoparticles arranged as regular shapes in the pyrolyzed HSS2T3 sample, but it is unclear if the arrangement is directly related to the regular polyhedral shapes of HKUST-1.

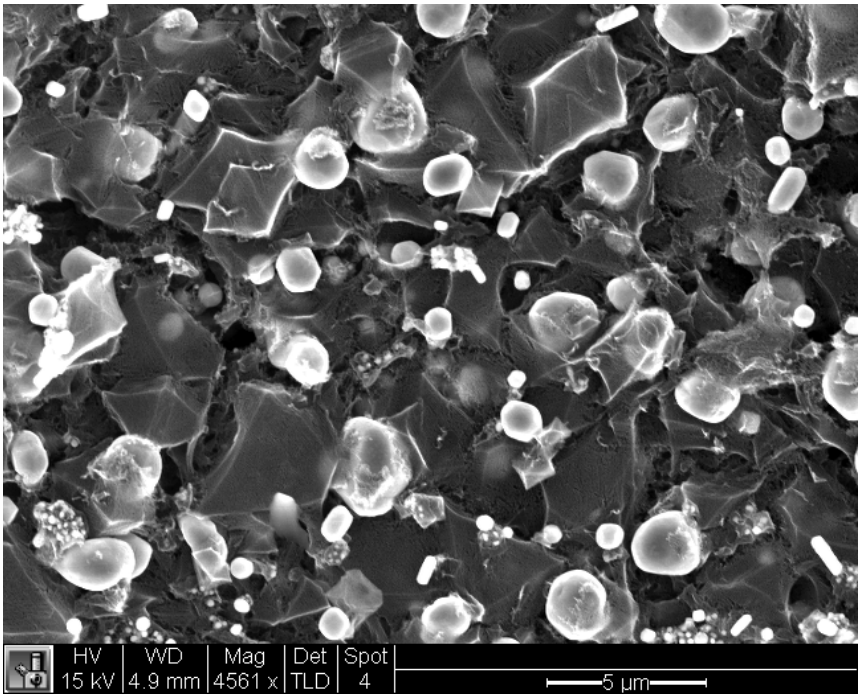


***Figure 10**. Pyrolyzed Cu anode after anodic deposition of HKUSt-1. Polyhedral carbon structures and Cu metal beads remain...*

## 6.5 Electrochemical Characteristics

CV of HSS1T3 indicates that it has less overpotential towards the vanadium positive electrode redox reactions, and is generally more reversible than ATCF and CF/PbO2. Comparison of its

peak current difference and peak current ratio corroborate this. Perhaps most notably, the cathodic reduction peak for the $V^{5+}/V^{4+}$ reaction occurs at a potential roughly 500mV higher than the other electrodes and has approximately twice the current density. There is also a plateau after each current peak in HSS1T3 at a voltage that potentially signifies another redox reaction taking place in addition to the vanadium redox reaction. Wu et al., have synthesized a $PbO_2$-coated carbon felt sample but its morphology is different from that of Method 1, and its peak ratio (~1.3) and peak difference (~0.5) are significantly higher than the case here, despite their lower scan rate. [52] This would suggest that morphology of the PbO2 coating affects it electrochemical performance as the VRFB positive electrode.

Unexpectedly, the electrode with the smallest peak separation is the pyrolyzed CF/PbO2 (M1Py) sample.

The onset potential for HSS1T3 occurs before that for M1Py, its peak currents are still much greater than those of M1Py, and the peak current ratio for HSS1T3 is still closest to 1. However, the CV curve suggest that the pyrolyzed $PbO_2$ serves a catalytic role for the vanadium redox reaction, while the addition of carbonized HKUST-1 improves charge transport. A comparison with pyrolyzed ATCF electrode, without any coating, must be done in order to see if is the lead species that is truly serving as a catalyst. In this regard, Melke *et al.* heat-treated carbon felt at 400 °C for 20 h, and CV of that electrode in the same VRFB solution showed similar, if not better, performance than M1Py. [53] So, it seems likely that part of the favorable performance of M1Py originates from its heat-treatment rather than any lead species on the surface. However, peak separation for the Melke group's electrode is about 0.3V for the 5 mV/s scan rate, with a peak current ratio of about 1.3, all of which are reversibility metric values that are less

favorable than those for HSS1T3. It must be determined if the higher heating temperature for the pyrolyzed electrodes presented here is at all related responsible for that comparative improvement.

Assuming the improvement comes from the presence of HKUST-1 derived carbon, there are some possibilities as to why that might be the case. It was suggested early on by Skyllas-Kazacos, and since largely accepted, that oxygen groups on the carbon surface play an important role as catalyst in the vanadium $VO^{2+}/VO_2^+$ redox reaction. [54] It is believed that $VO^{2+}$ in solution displace hydrogen ions from surface phenolic groups, electron transfer occurs along the resulting —C—O—V— bond, one oxygen is transferred from another nearby surface C—O group to V, and finally, the hydrogen ion from solution exchanges positions with the new $VO_2^+$ ion, which enters the bulk solution. There are 6 oxygen atoms from three carboxyl groups from each trimesic acid linker in HKUST-1. Determining how much of the oxygen remains after heating would be worthwhile because the remaining oxygens presumably can surface as catalyst sites. It has also been shown that a large degree of graphitic carbon with exposed edge sites (i.e., defects) can improve vanadium $VO^{2+}/VO_2^+$ redox kinetics. [55] Determining the concentration of edge defects for pyrolyzed HKUST-1 on the electrode would likely also prove fruitful. The loss of the polyhedral structure after pyrolysis suggests that a great deal of disorder is introduced into the carbon structure, which may lead to desirable exposed edge sites.

## 7. Conclusion & Future Work

Using peak differences and peak ratios as a metric, the electrochemical properties of the HSS1T3 electrode is comparable or better than several electrodes found literature, [56, 57, 58]

However, while it can be said that introduction of HKUST-1 as a carbon source positively affects the vanadium redox properties of the VRFB, the degree of contribution from the HKUST-1 structure has not been strictly determined.

To truly determine if HKUST-1 derived carbon coating on carbon felt improves vanadium redox, HKUST-1 must be directly grown onto carbon felt, instead of relying on the $PbO_2$ intermediary. HKUST-1 growth on glassy carbon has been demonstrated, after grafting carboxyphenol groups to the carbon surface or roughening the surface with abrasive paper. [59] Preliminary attempts to duplicate these processes were unsuccessful on carbon felt, but direct growth should be possible.

It has been demonstrated that the growth of certain crystallographic planes can be promoted during solvothermal synthesis of HKUST-1. [60] Forcing preferential growth of the 100 facets on the carbon substrate would allow one to take advantage of the larger crystal pore in that 100 plane. Presumably, because the MOF structure of HKUST-1 can be retained after pyrolysis, having more of the large pores of the 100 plane in contact with solution may access of the solvated vanadium ions to the electrode surface, but it may also allow exploration of its viability as a capacitor. This preferential growth was controlled using solvothermal synthesis, but no literature could be found about controlling facet growth during electrochemical deposition, which potentially offers shorter synthesis times and better scalability.

Lastly, it has been demonstrated introduction of nitrogen-containing functionals onto various carbon electrodes can enhance their properties and improve overall VRFB performance. [61, 62] Substituting amines onto the trimesic acid linker in HKUST-1 or simply depositing a nitrogen-containing MOF onto carbon felt before pyrolysis may allow integrated utilization of both the

robust MOF pore structure and the catalytic effect of nitrogen surface functionals towards better VRFB performance.

## Acknowledgements

Thank you to Professor Cao for his help and guidance during my research. Also, I am grateful for the help from Zachary Neale and Chaofeng Liu.

# References


[1] D. Kiron, N. Kruschwitz, K. Haanaes and I. Streng Velken, "Sustainability nears a tipping point," *MIT Sloan Management Review,* vol. 53, no. 2, pp. 69-74, 2012.

[2] United States Department of Energy, Office of Energy Efficiency & Renewable Energy, "2016-2020 Strategic Plan and Implementing Framework," United States Department of Energy, 2015.

[3] C. Quéré, R. Andrew, P. Friedlingstein, S. Sitch, J. Pongratz, A. Manning and J. Korsbakken, "Global carbon budget 2017," *Earth Syst. Sci. Data,* vol. 10, pp. 405-448, 2018.

[4] B. Dunn, H. Kamath and J.-M. Tarascon, "Electrical Energy Storage for the grid: a battery of choices," *Science,* vol. 334, no. 6058, pp. 928-935, 2011.

[5] P. J. Hall, M. Mirzaeian, F. S. I., F. Sillars, A. J. Rennie, G. O. Shitta-Bey, G. Wlson, A. Cruden and R. Carter, "Energy Storage in electrochemical capacitors: designing functional materials to improve performance," *Energ. Environ. Sci.,* vol. 3, no. 9, pp. 1238-1251, 2010.

[6] E. Sum and M. Skyllas-Kazacos, "A study of the V(II)/V(III) redox couple for redox flow cell applications," *J. Power Sources,* vol. 15, no. 2-3, pp. 179-190, 1985.

[7] M. Skyllas-Kazacos, M. Rychcik, R. Gt Robins, A. G. Fane and M. A. Green, "New all-vanadium redox flow cell," *J Electrochem Soc,* vol. 133, p. 1057, 1986.

[8] H. Furukawa, K. E. Cordova, M. O'Keefe and O. Yaghi, "The chemistry and applications of metal-organic frameworks," *Science,* vol. 341, no. 6149, p. 1230444, 2013.

[9] D. J. Tranchemontagne, Z. Ni, M. O'Keefe and O. M. Yaghi, "Reticular Chemistry of metal-organic polyhedra," *Angew. Chem., Int. Ed. Engl.,* vol. 47, no. 28, pp. 5136-5147, 2008.

[10] O. M. Yaghi and L. Hailan, "Hydrothermal synthesis of a metal-organic framework containing large rectangular channels," *J Amer Chem Soc,* vol. 117, no. 41, pp. 10401-10402, 1995.

[11] B. F. Hoskins and R. Robson, "Design and construction of a new class of scaffolding-like materials comprising infinite polymeric frameworks of 3D-linked molecular rods. A reappraisal of the zinc cyanide and cadmium cyanide structures and the synthesis and structure of [...]," *J Amer Chem Soc,* vol. 112, no. 4, pp. 1546-1554, 1990.

[12] S. Kitagawa, S. Matsuyama, M. Munakata and T. Emori, "Synthesis and crystal structures of novel one-dimensional polymers,[{M (bpen) X}∞][M= Cu I, X= PF 6–; M= Ag I, X= ClO 4–; bpen= trans-1, 2-bis (2-pyridyl) ethylene] and [{Cu (bpen)(CO)(CH 3 CN)(PF 6)}∞]," *J Amer Chem Soc, Dalton Trans,* vol. 11, pp. 2869-2874, 1991.

[13] M. O'Keefe and O. Yaghi, "Deconstructing the Crystal Structures of Metal-Organic Frameworks and Related Materials into Their Underlying Nets," *Chem Rev,* vol. 112, pp. 675-702, 2011.

[14] I. M. Hönicke, I. Senkovska, V. Bon, I. Baburin, N. Bönisch, S. Raschke, J. Evans and S. Kaskel, "Balancing Mechanical Stability and Ultrahigh Porosity in Crystalline Framework Materials," *Angew Chem Int,* vol. 57, no. 42, pp. 13780-13783, 2018.

[15] H. Li, K. Wang, Y. Sun, C. Lollar, J. Li and H.-C. Zhou, "Recent advances in gas storage and separation using metal-organic frameworks," *Mater Today,* vol. 21, no. 2, pp. 108-121, 2018.

[16] P. Küsgens, M. Rose, I. Senkovska, H. Fröde, A. Henschel and S. Siegle, "Characterization of metal-organic frameworks by water adsorption," *Microporous Mesoporous Mater,* vol. 120, pp. 325-330, 2008.

[17] J. Low, A. Benin, P. Jakubczak, J. Abrahamian, S. Faheem and R. Willis, "Virtual High Throughput Screening Confirmed Experimentally: Porous Coordination Polymer Hydration," *J Amer Chem Soc,* vol. 131, no. 43, pp. 15834-15842, 2009.

[18] H. Furukawa, Y. B. Go, N. Ko, Y. K. Park, F. J. Uribe-Romo, J. Kim, M. O'Keeffe and O. Yaghi, "Isoreticular Expansion of Metal-Organic Frameworks with Triangular and Square Building Units and the Lowest Calculated Density for Porous Crystals," *Inorg Chem,* vol. 50, no. 18, pp. 9147-9152, 2011.

[19] S. Cohen, "Modifying MOFs: new chemistry, new materials," *Chem Sci,* vol. 1, pp. 32-36, 2010.

[20] Y.-F. Niu, W. Zhao, J. Han, G. Tian and X.-L. Zhao, "Unprecedented metal-ion metathesis in a metal-carboxylate chain-based metal-organic framework," *CrystEngComm,* vol. 16, no. 12, pp. 2344-2347, 2014.

[21] M. Kim, J. F. Cahill, H. Fei, K. Prather and S. Cohen, "Postsynthetic Ligand and Cation Exchange in Robust Metal-Organic Frameworks," *J Amer Chem Soc,* vol. 134, no. 43, pp. 18082-18088, 2012.

[22] K. Qi, R. Hou, S. Zaman, Y. Qiu, B. Y. Xia and H. Duan, "Contruction of Metal-Organic Framework/Conductive Polymer Hybrid for All-Solid-State Fabric Supercapacitor," *ACS Appl Mater Interfaces,* vol. 10, pp. 18021-18028, 2018.

[23] F. Zhang, Y. Wang, T. Chu, Z. Wang, W. Li and Y. Yang, "A facile fabrication of electrodeposited luminescent MOF thin films for selective and recyclable sensing fo nitroaromatic explosives," *Analyst,* vol. 141, pp. 4502-4510, 2016.

[24] A. Centrone, T. Harada, S. Speakman and T. A. Hatton, "Facile Synthesis of Vanadium Metal-Organic Frameworks and their Magnetic Properties," *Small,* vol. 6, no. 15, pp. 1598-1602, 2010.

[25] M. Glavinović, F. Qi, A. Katsenis, T. Friščić and J.-P. Lumb, "Redox-promoted associative assembly of metal-organic materials," *Chem Sci,* vol. 7, pp. 707-712, 2016.

[26] D. DeSantis, J. Mason, B. James, C. Houchins, J. Long and M. Veenstra, "Techno-economic Analysis of Metal-Organic Frameworks for Hydrogen and Natural Gas Storage," *Energy Fuels,* vol. 31, pp. 2024-2032, 2017.

[27] U. Mueller, M. Schubert, F. Teich, H. Puetter, K. Schierle-Arndt and J. Pastré, "Metal-organic frameworks—prospective industrial applications," *J Mater Chem,* vol. 16, pp. 626-636, 2006.

[28] M. Gaab, T. Natalia, M. Stefan, R. Gummaraju and U. Müller, "The progression of Al-based metal-organic frameworks—From academic research to industrial production and applications," *Microporous Mesoporous Mater,* vol. 157, pp. 131-136, 2012.

[29] C. Young, R. Salunkhe, J. Tang, C.-C. Hu, M. Shahabuddin, E. Yanmaz, M. S. A. Hossain, J. H. Kim and Y. Yamauchi, "Zeolitic imidazolate framework (ZIF-8) derived nanoporous carbon: the effect of carbonization temperature on the supercapacitor performance in an aqueous electrolyte," *Phys Chem Chem Phys,* vol. 18, pp. 29308-29315, 2016.

[30] M. Skyllas-Kazacos, L. Cao, M. Kazacos, N. Kausar and A. Mousa, "Vanadium Electrolyte Studies for the Vanadium Redox Battery—A Review," *ChemSusChem,* vol. 9, pp. 1521-1543, 2016.

[31] C. Ponce de León, A. Frías-Ferrer, J. González-García, D. A. Szánto and F. C. Walsh, "Redox flow cells for energy conversion," *J Power Sources,* vol. 160, pp. 716-732, 2006.

[32] J. Kim, H. Lim, J.-Y. Jyoung, E.-S. Lee, J. S. Yi and D. Lee, "Effects of Doping Methods and Kinetic Relevance of N and O Atomic Co-Functionalization on Carbon Electrode for V(IV)/V(V) Redox Reactions in Vanadium Redox Flow Battery," *Electrochim Acta,* vol. 245, pp. 724-733, 2017.

[33] Z. Jiang, K. Klyukin and V. Alexandrov, "First-principles study of adsorption-desorption kinetics of aqueous V2+/V3+ redox species on graphite in a vanadium redox flow battery," *Phys Chem Chem Phys,* vol. 19, pp. 14897-14901, 2017.

[34] C. Schmidt and G. Cao, "Properties of mesoporous carbon modified carbon felt for anode of all-vanadium redox flow battery," *Sci China Mater,* vol. 59, no. 12, pp. 1037-1050, 2016.

[35] P. C. Lemaire, J. Zhao, P. S. Williams, H. J. Walls, S. D. Shepherd, M. D. Losego, G. W. Peterson and G. N. Parsons, "Copper benzenetricarboxylate metal-organic framework nucleation mechanisms on metal oxide powders and thin films formed by atomic layer deposition.," *ACS Appl Mater Interfaces,* vol. 8, no. 14, pp. 9514-9522, 2016.

[36] B. H. Toby and R. B. Dreele, "GSAS-II: the genesis of a modern open-source all purpose crystallography software package," *J. Appl. Crystallogr.,* vol. 46, no. 2, pp. 544-549, 2013.

[37] C. Wang, Q. Xueren and A. Xianhui, "In situ green preparation and antibacterial activity of copper-based metal-organic frameworks/cellulose fibers (HKUST-1/CF) composite," *Cellulose,* vol. 22, no. 6, pp. 3789-3797, 2015.

[38] A. J. Bard and L. R. Faulkner, Electrochemical methods: fundamentals and applications, New York: Wiley, 2001.

[39] C. Flox, M. Skoumal, J. Rubio-Garcia, T. Andreu and J. R. Morante, "Strategies for enhancing electrochemical activity of carbon-based electrodes for all-vanadium redox flow batteries," *Appl Energy,* vol. 109, pp. 344-351, 2013.

[40] K. J. Kim, Y. J. Kim, J. H. Kim and M. S. Park, "The effects of surface modifications on carbon felt electrodes for use in vanadium redox flow batteries," *Mater Chem Phys,* vol. 131, no. 1-2, pp. 547-553, 2011.

[41] J. Langer, M. Bruns, D. Dixon, A. Nefedov, C. Wöll, F. Scheiba, H. Ehrenberg, C. Roth and J. Melke, "Surface properties and graphitization of polyacrylonitrile based fiber electrodes

affecting the negative half-cell reaction in vanadium redox flow batteries," *J Power Sources,* vol. 321, pp. 210-218, 2016.

[42] B. Sun and M. Skyllas-Kazacos, "Chemical Modification of graphite electrode materials for vanadium redox flow battery application—part II. Acid treatments," *Electrochim Acta,* vol. 37, no. 13, pp. 2459-2465, 1992.

[43] J. Zhao, M. D. Losego, P. C. Lemaire, P. S. Williams, B. Gong, S. E. Atanasov, T. M. Blevins, C. J. Oldham, H. J. Walls, S. D. Shepherd and M. A. Browe, "Highly Adsorptive, MOF-Functionalized Nonwoven Fiber Mats for Hazardous Gas Capture Enabled by Atomic Layer Deposition," *Adv Mater Interfaces,* vol. 1, no. 4, p. 1400040, 2014.

[44] M. Kosmulski, "Isoelectric points and points of zero charge of metal (hydr)oxides: 50 years after Parks' review," *Adv Colloid Interface Sci,* vol. 238, pp. 1-61, 2016.

[45] M. Li and M. Dincă, "Reductive electrosynthesis of crystallline metal-organic frameworks," *J Amer Chem Soc,* vol. 133, no. 33, pp. 1296-12929, 2011.

[46] M. Li and M. Dincă, "On the Mechanism of MOF-5 Formation under Cathodic Bias," *Chem Mater,* vol. 27, no. 9, pp. 3203-3206, 2015.

[47] R. Ameloot, L. Stappers, J. Fransaer, L. Alaerts, B. F. Sels and D. E. De Vos, "Patterned growth of metal-organic framework coatings by electrochemical synthesis," *Chem Mater,* vol. 21, no. 13, pp. 2580-2582, 2009.

[48] T. R. Van Assche, G. Desmet, R. Ameloot, D. E. De Vos, H. Terryn and J. F. Denayer, "Electrochemical Synthesis of thin HKUST-1 layers on copper mesh," *Microporous Mesoporous Mater,* vol. 158, pp. 209-213, 2012.

[49] N. Campagnol, T. R. Van Assche, M. Li, L. Stappers, M. Dincă, J. F. Denayer, K. Binnemans, D. E. De Vos and J. Fransaer, "On the electrochemical deposition of metal-organic frameworks," *J Mater Chem,* vol. 4, no. 10, pp. 3914-3925, 2016.

[50] Y. Wang, J. Wu, Z. Wang, A. Terenyi and D. E. Giammar, "Kinetics of lead(IV) oxide (PbO2) reductive dissolution: Role of lead (II) adsorption and surface speciation," *J Colloid Interface Sci,* vol. 389, no. 1, pp. 236-243, 2013.

[51] Y. Song, D. Cho, S. Venkateswarlu and M. Yoon, "Systematic study on preparation of copper nanoparticle embedded porous carbon by carbonization of metal-organic framework for enzymatic glucose sensor," *RSC Adv,* vol. 7, pp. 10592-10600, 2017.

[52] X. Wu, H. Xu, L. Lu, H. Zhao, J. Fu, Y. Shen, P. Xu and Y. Dong, "PbO2-modified graphite felt as the positive electrode for an all-vanadium redox flow battery," *J Power Sources,* vol. 250, pp. 274-278, 2014.

[53] J. Melke, P. Jakes, J. Langner, L. Riekehr, U. Kunz, Z. Zhao-karger, A. Nefedov, H. Sezen, C. Wöll, H. Ehrenberg and C. Roth, "Carbon materials for the positive electrode in all-vanadium redox flow batteries.," *Carbon,* vol. 78, pp. 220-230, 2014.

[54] B. Sun and M. Skyllas-Kazacos, "Modification of graphite eletrode materials for vanadium redox flow battery application—I. Thermal treatment," *Electrochim Acta,* vol. 37, no. 7, pp. 1253-1260, 1992.

[55] H. Liu, L. Yang, Q. Xu and C. Yan, "An electrochemically activated graphite electrode with excellent kinetics for electrode processes of V(II)/V(III) and V(IV)/V(V) couples in a vanadium redox flow battery," *RSC Adv,* vol. 4, pp. 55666-55670, 2014.

[56] K. J. Kim, H. S. Lee, J. Kim, M.-S. Park, J. H. Kim, Y.-J. Kim and M. Skyallas-Kazacos, "Superior electrocatalytic activity of a robust carbon-felt electrode with oxygen-rich phosphate groups for all-vanadium redox flow batteries," *ChemSusChem,* vol. 9, no. 11, pp. 1329-1338, 2016.

[57] Y. Liu, Y. Shen, L. Yu, L. Liu, F. Liang, X. Qiu and J. Xi, "Holey-engineered electrodes for advanced vanadium flow batteries," *Nano Energ,* vol. 43, pp. 55-62, 2018.

[58] C. Su, Y. Zhao and J. Xi, "Phosphorous-doped carbon nitride as powerful electrocatalyst for high-power vanadium flow battery," *Electrochim Acta,* vol. 286, pp. 22-28, 2018.

[59] S. Balakrishnan, A. J. Downward and S. G. Telfer, "HKUST-1 growth on glassy carbon," *J Mater Chem,* vol. 21, no. 48, pp. 19207-19209, 2011.

[60] Z. Wang, L. Ge, M. Li, R. Lin, H. Wang and Z. Zhonghua, "Oriented growht of copper-based MOF for acetylene storage," *Chem Eng J,* vol. 357, pp. 320-327, 2019.

[61] S. Park and H. Kim, "Fabrication of nitrogen-doped graphite felts as positive electrodes using polypyrrole as a coating agent in vanadium redox flow batteries," *J Mater Chem A,* vol. 3, pp. 12276-12283, 2015.

[62] M. Park, J. Ryu, Y. Kim and J. Cho, "Corn protein-derived nitrogen-doped carbon materials with oxygen-rich function groups: a highly efficient electrcatalyst for all-vanadium redox flow batteries," *Energ Environ Sci,* vol. 7, pp. 3727-3735, 2014.